Ecological Informatics 93 (2026) 103558

Contents lists available at ScienceDirect

Ecological Informatics

journal homepage: www.elsevier.com/locate/ecolinf

Deep learning-based canopy gap detection using a cross-technological approach with airborne laser scanning and aerial imagery data

Florian Franz [a,b,*], Dominik Seidel [b], Philip Beckschäfer [a]

[a] Northwest German Forest Research Institute, Section Remote Sensing and GIS, Grätzelstraße 2, 37079 Göttingen, Germany
[b] University of Göttingen, Department for Spatial Structures and Digitization of Forests, Büsgenweg 1, 37077 Göttingen, Germany

ARTICLE INFO

Keywords:
Canopy gap detection
Deep learning
Airborne laser scanning
Digital aerial photogrammetry

ABSTRACT

Canopy gaps are crucial structural elements of forests, supporting biodiversity and influencing forest dynamics and ecosystem health. Airborne laser scanning (ALS) is commonly used for forest gap analysis and typically outperforms digital aerial photogrammetry (DAP), especially in detecting smaller gaps. However, ALS data availability remains limited compared to DAP. Given the broader availability and cost-effectiveness of DAP, this study aimed to overcome its technical drawbacks in canopy gap detection by applying a cross-technological approach with multiple data sources. This involves ALS-derived reference data fused with spectral and height information from DAP. We developed a deep learning-based method, employing a convolutional neural network (CNN), specifically the U-Net architecture, for detecting canopy gaps. The U-Net was trained using gap polygons automatically generated from ALS-derived canopy height models (CHMs), combined with true digital orthophotos (TDOPs) and DAP-based CHMs. Adding spectral information from TDOPs was intended to help detect shadows typically associated with smaller canopy gaps, which are often missed in DAP-based CHMs. The model was tested in the Solling, a forest area in a low mountain range in Central Germany. Performance was evaluated in independent test areas representing a gradient of structural heterogeneity. Overall, our model achieved moderate to high segmentation performance (IoU: 0.67–0.77; F1-score: 0.56–0.74). Once trained, it can be applied to image-derived inputs, improving canopy gap detection F1-score by on average 0.08 compared to using DAP-based CHMs alone. Our results demonstrate a novel approach for detecting canopy gaps without ALS data, suggesting applications across broader spatial and temporal scales.

1. Introduction

Canopy gaps are a characteristic structural element of many of the world's forests, developing e.g. after natural disturbances such as storms, insect infestations, or fires (Jucker, 2022; Muscolo et al., 2014; Schliemann and Bockheim, 2011) or simply through natural tree mortality. There is no universally accepted definition of what a "canopy gap" is (Jucker, 2022). In the most general sense, gaps can be described as openings in the canopy caused by treefall (Schliemann and Bockheim, 2011), forming an integral part of natural forest dynamics (Runkle, 1982; Watt, 1947; Whitmore, 1989).

Within canopy gaps, environmental conditions usually differ from those of the surrounding forest, e.g., in terms of light availability, temperature, soil moisture, and nutrients (de Freitas and Enright, 1995; Horváth et al., 2023; Hou et al., 2024; Ritter et al., 2005). Depending on the size of the gap, the gap-specific microclimate influences upcoming tree species composition inside the gap as part of natural regeneration processes (Bagnato et al., 2021; Nagel et al., 2010; Vodde et al., 2015). According to the gap partitioning hypothesis (Denslow, 1980), resources for tree regeneration are distributed diversely in canopy gaps, enabling the coexistence of trees with different survival strategies (Kern et al., 2013). Besides tree species composition, also animal species composition is influenced by canopy openings, as shown, e.g., for insects (Eckerter et al., 2021) or birds (Pollock et al., 2020). Biodiversity generally tends to increase after gap formation due to increased structural heterogeneity of otherwise closed canopy forests (Heidrich et al., 2020; Schall et al., 2018). Considering this, harvesting regimes have been developed that try to mimic natural disturbances (Gustafsson et al., 2020; Kuuluvainen et al., 2021; Mason et al., 2022), aiming to restore more structurally diverse forests including canopy gaps (Muscolo et al., 2014).

Therefore, knowledge of the spatial distribution of gaps in forest

* Corresponding author at: Northwest German Forest Research Institute, Section Remote Sensing and GIS, Grätzelstraße 2, 37079 Göttingen, Germany.
E-mail address: florian.franz@nw-fva.de (F. Franz).

https://doi.org/10.1016/j.ecoinf.2025.103558
Received 30 May 2025; Received in revised form 8 December 2025; Accepted 9 December 2025
Available online 12 December 2025

stands is important for forest management and monitoring purposes. In particular, studying the gap development processes over time, including gap formation, expansion, shrinking, and closure, offers the opportunity to understand the dynamics that shape forest structure, biodiversity, and ecosystem function (Jucker, 2022; McCarthy, 2001). Early research on canopy gaps and their dynamics was performed by measuring and mapping them in the field using definitions suggested by different ecologists (Runkle, 1992). Such terrestrial studies are still conducted today (e.g. Feldmann et al., 2018). However, manually mapping canopy gaps in the field is very time consuming. As an alternative, remote sensing has emerged as a valuable technology for the assessment of canopy gaps (St-Onge et al., 2014).

Numerous remote sensing technologies were employed to study canopy gaps, ranging from satellite images (Dalagnol et al., 2019; Garbarino et al., 2012; Hobi et al., 2015; Lassalle and de Souza Filho, 2022), aerial images (Nyamgeroh et al., 2018), and uncrewed aerial vehicle (UAV) images (Chen et al., 2023; Getzin et al., 2014; Htun et al., 2024; Xia et al., 2022) to airborne laser scanning (ALS) (Asner et al., 2013; Dalagnol et al., 2021; Goodbody et al., 2020; Gorgens et al., 2023; Hagemann et al., 2022; Krüger et al., 2024; Reis et al., 2022; Vepakomma et al., 2008), UAV laser scanning (Chung et al., 2022), and terrestrial laser scanning (Seidel et al., 2015). In image-based studies, methods involve visual image interpretation and manual delineation of gaps (e.g. Hobi et al., 2015), as well as automated tracking of gaps (Lassalle and de Souza Filho, 2022; Seidel et al., 2015). In contrast, laser scanning-based investigations rely on the technology's ability to automatically identify gaps by detecting canopy height deviations between gaps and the surrounding forest (St-Onge et al., 2014). ALS is the most widely used technique due to its objectivity and accuracy in measuring three-dimensional forest structures over large areas (Jucker, 2022). The accuracy and reliability of ALS-based canopy heights have established this technology as the standard for evaluating gap detection methodologies (Dietmaier et al., 2019; White et al., 2018), and tools designed for forest gap analysis with ALS-derived canopy height models (CHMs) have been developed (Silva et al., 2019). Image-based CHMs, derived via digital aerial photogrammetry (DAP), are however a cost-effective alternative to ALS (Goodbody et al., 2019) and studies have highlighted the potential of using photogrammetric height data to detect canopy gaps (Renaud et al., 2017; Solano et al., 2022; Zielewska-Büttner et al., 2016a). Two comparative analyses (Dietmaier et al., 2019; White et al., 2018) revealed a better performance of ALS CHMs for accurately mapping forest canopy gaps, especially regarding small canopy openings, which frequently occur in mature and old-growth forest stands. The detection of those smaller gaps is often not possible based on DAP-derived CHMs, as these tend to be inaccurate in dark shadow areas, frequently occurring in gaps (White et al., 2018; Zielewska-Büttner et al., 2016a).

Nevertheless, considering the lower cost of aerial imagery and their prevailing frequent and wide availability compared to ALS data, methods to accurately detect canopy gaps in DAP-derived CHMs would be beneficial.

The aim of this study was to overcome the technical drawbacks of DAP-derived CHMs regarding canopy gap detection and to develop an image-based method for accurately mapping canopy gaps. Therefore, we applied a cross-technological approach with multiple data sources in which ALS-derived canopy gaps provide the reference for training and validation of a convolutional neural network (CNN) to detect canopy gaps based on true digital orthophotos (TDOPs) and DAP-derived CHMs. The idea of combining the DAP-derived CHM with the TDOP was to equip the CNN with spectral information that allows for the identification of shadows, which usually characterize smaller canopy gaps that would otherwise not be detected using DAP-derived CHMs alone.

2. Materials and methods

2.1. Study area

This study was conducted in the Solling region (Fig. 1), a low mountain range in Central Germany where elevations range up to 527 m a.s.l. The area is characterized by temperate forests, although large areas are also dominated by the boreal coniferous tree species Norway spruce (*Picea abies* (L.) Karst.). European beech (*Fagus sylvatica* L.) is the second most frequent tree species in the area. Other tree species, such as Scots pine (*Pinus sylvestris* L.), Douglas fir (*Pseudotsuga menziesii* (Mirbel) Franco), European larch (*Larix decidua* Mill.), and oak (*Quercus robur* L., *Quercus petraea* (Mattuschka) Liebl.) are occasionally found. The forests in this area have historically undergone intensive management, leading to the establishment of extensive pure spruce stands. In recent decades, the region has experienced disturbances from wind-throw and bark beetles, affecting large areas of spruce forest. As a result, many stands are now undergoing conversion into more structurally diverse mixed forests. These disturbances, along with selective logging, contribute to the heterogeneous forest structure typical of Central European forests.

2.2. Data acquisition and pre-processing

We used data from an aerial survey carried out in September 2023. Digital aerial images and ALS point clouds were acquired in one overflight (duration of two days) with a UltraCamEagle M1 camera system and a VQ-780II-S Riegl Lascerscanner. The aerial images have four spectral bands (RGB and NIR) with a ground sampling distance (GSD) of 0.05–0.08 m, taken with an overlap of at least 80 % along-track and 66 % across-track. The point density of the ALS point cloud was at least 16 points m^{-2}. Mean flight height during the survey was 1290 m a.s.l. Further acquisition parameters can be found in Table 1.

The pre-processing of the ALS point clouds was primarily conducted using the *lasR* package (Roussel, 2024) in R 4.4.0 (R Core Team, 2024). However, the classification into ground points and non-ground points was done using the *lasground_new* function from LAStools (version 230330) (Rapidlasso GmbH, 2021), as this specific algorithm is not available in *lasR* and performed well with our data. The classified point clouds were normalized with a triangulation of the ground points. After this, two filters were applied: The first filter removed points above 55 m and below −1 m, as those were considered outliers. The second filter dropped remaining points classified as 'noise' using an isolated voxel filter, as implemented in the *lasR* package (resolution of the voxels: 5 m, maximal number of points: 6). Subsequently, resampling to 0.5 m resolution CHMs raster files was done using the highest point per pixel (point-to-raster method). Finally, pits and spikes were filled in the CHMs and the *merge* function (*terra* package (Hijmans, 2024)) was used to generate one single CHM raster file from all individual CHM tiles.

The photogrammetric workflow for processing the aerial images entailed the orientation of the images, their orthorectification, and dense-image-matching to generate 3D point clouds. Oriented images and TDOPs were provided by the State Office for Geoinformation and Surveying of Lower Saxony (Landesamt für Geoinformation und Landesvermessung Niedersachsen). Image-matching was done in *Trimble/Inpho* software MATCH-T DSM (version 9.2). The integrated matching strategy is a combination of semi-global-matching and feature-based-matching executed on different pyramid levels (Trimble, 2019). We started by setting the pyramid level to 10 for the matching process and subsequently used three different last pyramid levels (2, 1, and 0). This resulted in point densities of 11–18 points m^{-2} for level 2, 45–69 points m^{-2} for level 1, and 180–275 points m^{-2} for level 0. All point clouds were afterwards thinned to a point density of 4 points m^{-2} to reduce file size by selecting the highest point within a grid cell of 0.5 m resolution. Corresponding to the initial point densities, the thinned point clouds and resulting digital surface models (DSMs) were of differing quality, regarding the depiction of crown shapes and the amount of noise pixels.

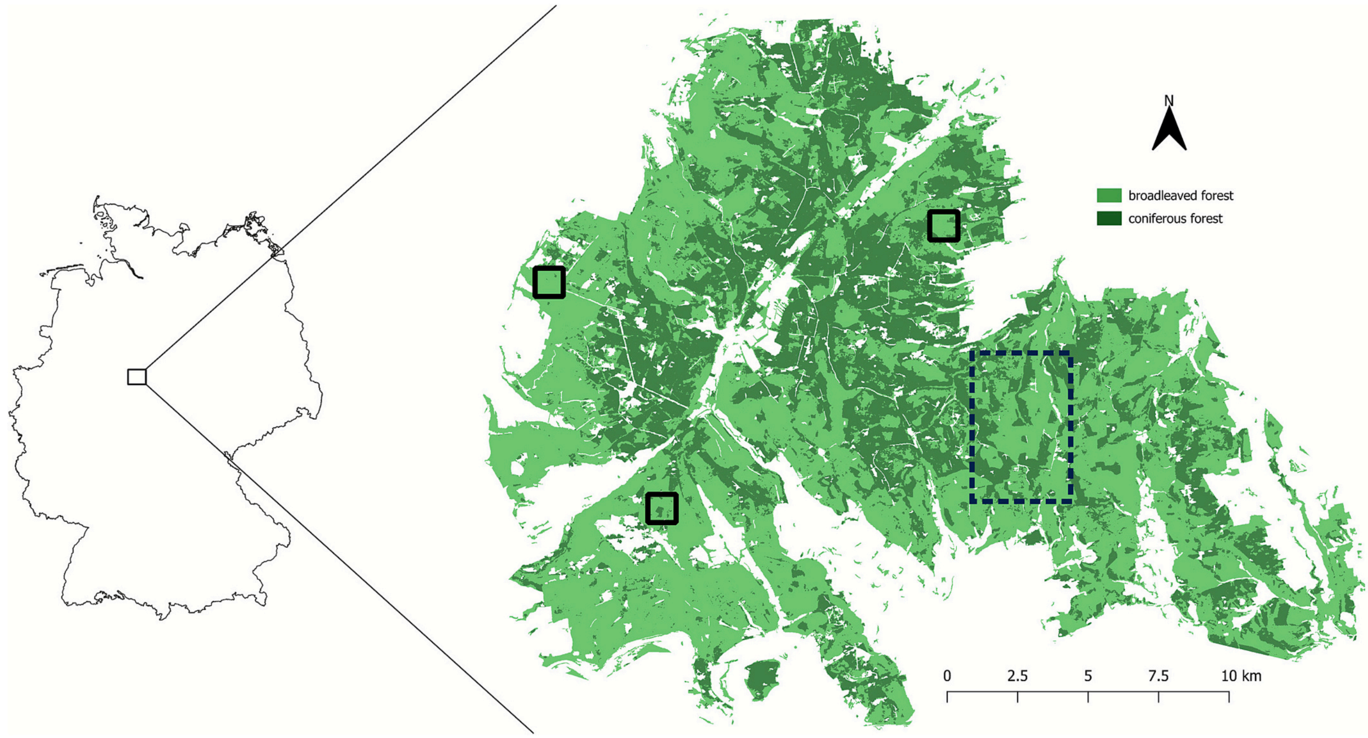

Fig. 1. Location of the Solling area in Germany with its main forest types. Rectangles represent the training area (dot line) and testing areas (solid line) described in Section 2.4. Germany borders: © BKG (2024) dl-de/by-2-0, forest types: © EEA (2020).

Table 1
Acquisition parameters of the imagery and LiDAR (Light Detection and Ranging) survey.

Parameter	Description
Mean flight height	1290 m a.s.l.
Mean aircraft speed	240 km h^{-1}
Flight dates	4 Sep. 2023 (train area, test area 1 and 3) 5 Sep. 2023 (train area, test area 2)
Overall duration of the flight	11:15 h
Camera: UltraCamEagle M1	
- Focal length	100.5 mm
- Spectral resolution	four-band (RGB and NIR)
- GSD	0.05–0.08 m
- Overlap	80 % / 66 %
- Pixel size	5.2 µm
LiDAR-sensor: VQ-780II-S Riegl	
- Scan angle	± 20°
- Mean swath width	939 m
- Mean swath overlap	~61 %
- Pulse repetition rate	933 kHz
- Scan frequency	210 Hz
- Point density	min. 16 points m^{-2}

We did this, to test for the model's applicability to image-based CHMs of varying quality. Using an ALS-based digital terrain model, these DSMs were eventually normalized using a digital terrain model and filtered similarly to the ALS-based point clouds to generate DAP-based CHM raster files in 0.5 m resolution.

2.3. Gap detection in ALS-based CHMs

Several gap detection approaches have been applied in studies on canopy gap detection utilizing ALS. They can be divided into methods with fixed or variable height thresholds, whereby the first is set to a single value by the user while the second is variable as it considers the tree heights surrounding a gap (White et al., 2018). The criteria to define a gap, such as the maximum vegetation height inside the gap or the gap area, vary substantially in the literature; a common definition is lacking (Jucker, 2022). For our study, we defined gaps as follows: A gap is an area of 10 to 5000 m^2 on which the trees are only half as high as the trees surrounding the gap.

The minimum area was set to 10 m^2, a compromise between potentially noise gaps and small openings, which are particularly common in temperate natural deciduous forests (Drößler and von Lüpke, 2005). The maximum gap area was set to 5000 m^2 to exclude open areas that lack typical forest gap characteristics. Three different thresholds (5 m, 10 m, and 15 m) were chosen for the maximum vegetation height inside a gap. For each height threshold, the vegetation surrounding a gap within a 20 m buffer should always be twice the maximum vegetation height inside the gap, with at least 75 % of the values within the buffer exceeding this threshold. This led us to create three height stages: 5 m inside the gap, 10 m within the buffer; 10 m inside the gap, 20 m within the buffer; 15 m inside the gap, 30 m within the buffer. By doing this, we ensure a clear distinction between a gap and its surrounding trees corresponding to a sharp breach in the surface of the canopy (St-Onge et al., 2014).

The *ForestGapR* package (Silva et al., 2019) was used to automatically detect gaps based on the three different vegetation height thresholds inside the gap. The lowest value (5 m) corresponds to the minimum tree height at which vegetation can be considered a forest according to the FAO definition (FAO, 2020). The canopy gaps were detected for each vegetation height threshold with the area sizes mentioned above. Subsequently, the gaps were filtered by creating the 20 m buffer around each gap. The 25th percentile was calculated to ensure that at least 75 % of the values within the buffer exceeded a certain canopy height, corresponding to twice the maximum vegetation height inside the gap.

2.4. Training and test dataset preparation

For model training, an area of 1837.5 ha located in the eastern part of the study area was used (Fig. 1). The TDOP was downsampled from 0.07 m to 0.5 m to match the resolution of the CHMs and normalized to a value range of 0–255 (conversion from 16 bit to 8 bit). The CHM was computed in three different quality levels with each covering only a third of the training area. Hence, the three CHMs were mosaicked to cover the whole training area before they were stacked to the four spectral bands of the TDOP. For technical reasons of model training, the ALS-based detected canopy gaps as raster mask (0 = non-gap, 1 = gap) were also stacked to the same file (Fig. 2).

To test our model, three areas of size 1 × 1 km were selected from the study region (Fig. 1). These test areas were deliberately chosen based on visual aspects to represent a diverse range of forest structures and illumination conditions. The forest type composition of the training and test areas, derived from the forest type layer shown in Fig. 1, is provided in Table 2. The test datasets were generated as previously described for the training dataset. According to the three different pyramid levels and resulting CHMs, three test datasets were created per area (Fig. 3) to examine if the point density and thereof derived CHM quality influences model prediction.

Table 2
Forest type composition in training and test areas. Remaining pixels represent non-forest areas.

Area	Broadleaved (%)	Coniferous (%)
Training area	61	36
Test area 1	77	22
Test area 2	87	12
Test area 3	96	2

2.5. Model training and evaluation

We employed a U-Net, a CNN architecture first introduced by

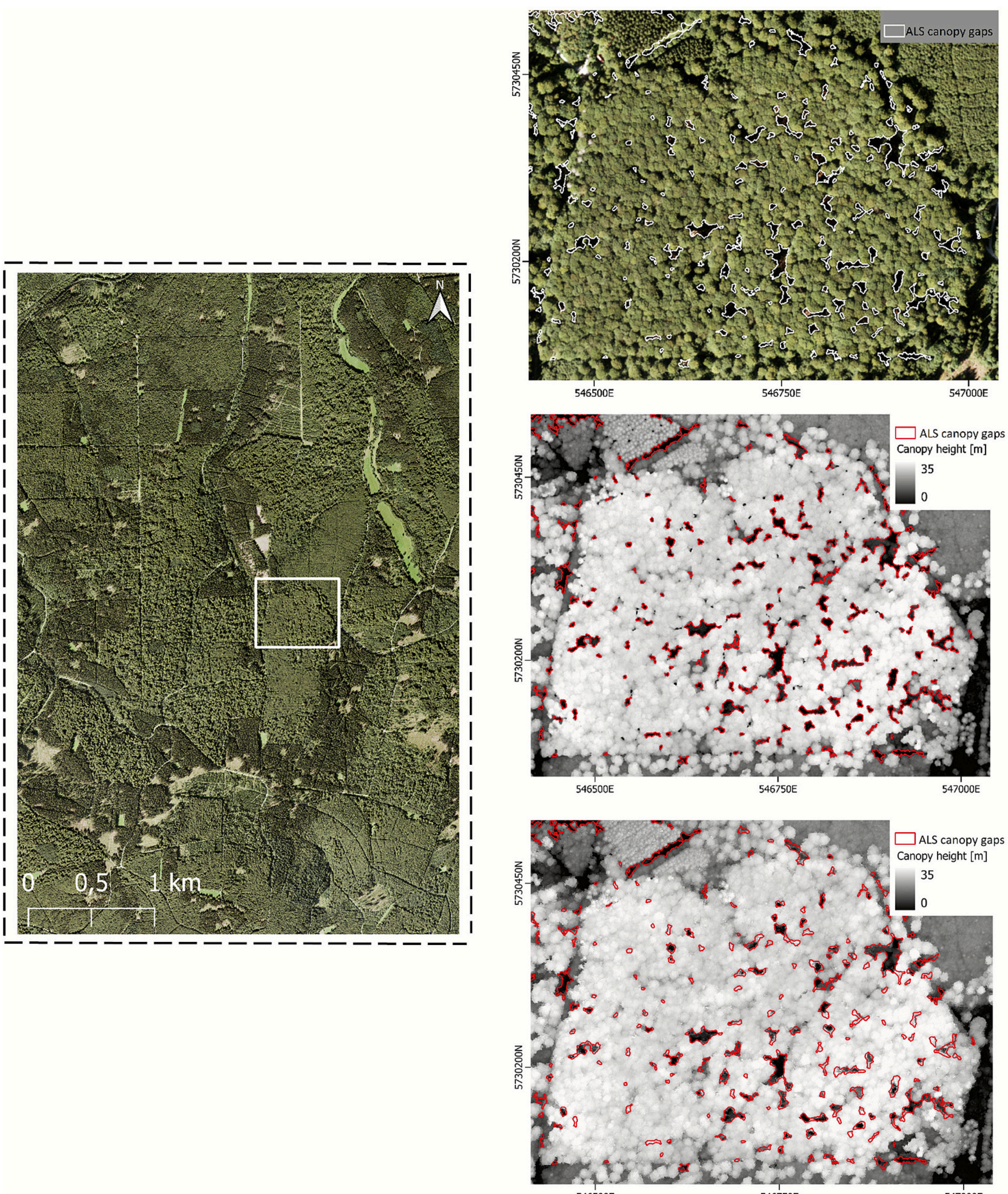

Fig. 2. RGB true digital orthophoto (RGB-TDOP) of the whole training area (left) and zoomed-in subarea (white rectangle): RGB-TDOP (top right), airborne laser scanning (ALS)-based canopy height model (CHM) (center right), and digital aerial photogrammetry (DAP)-based CHM (bottom right). All displayed canopy gaps (here as polygons) were derived from the ALS-CHM.

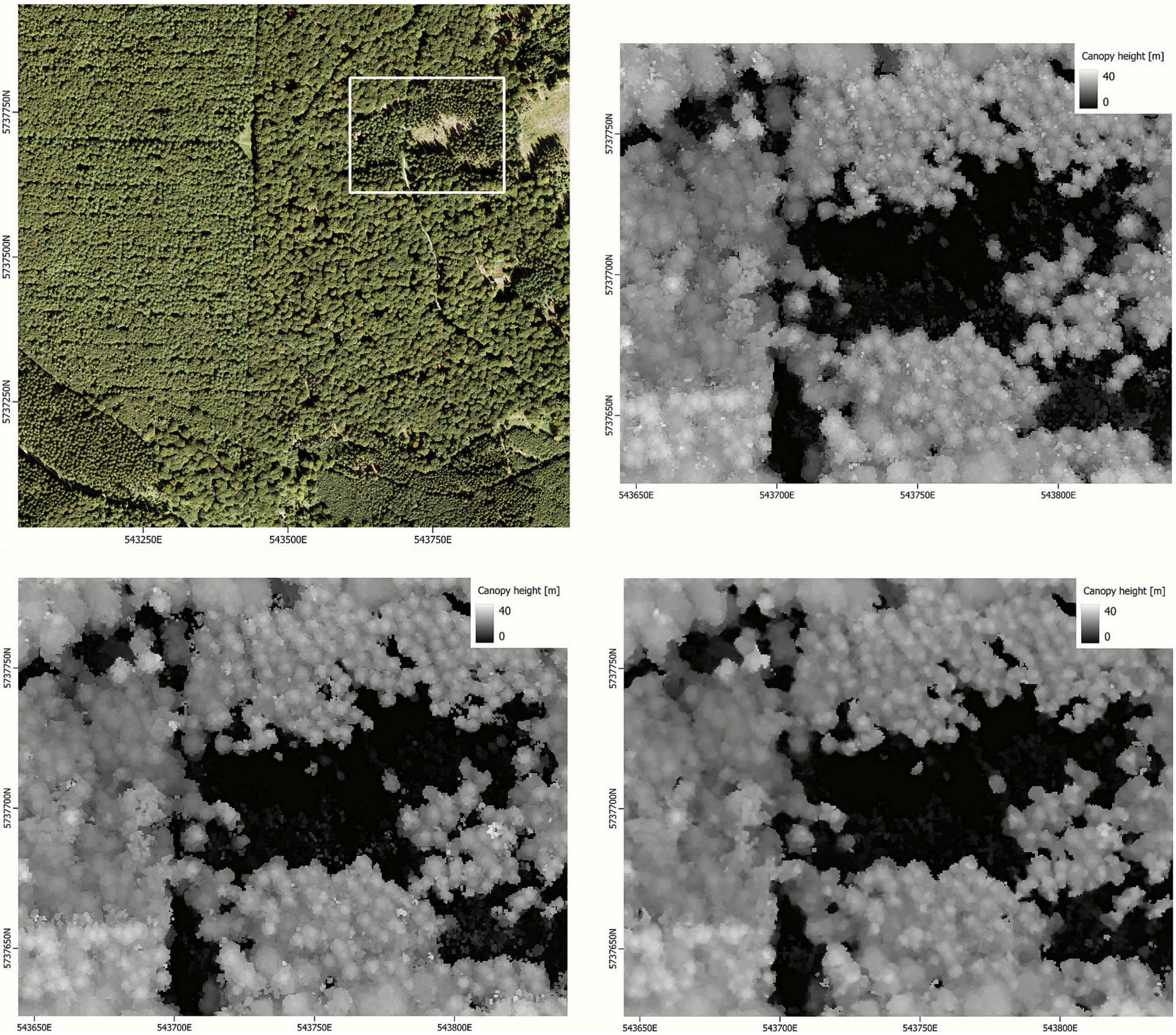

Fig. 3. Example test area: RGB true digital orthophoto (RGB-TDOP) (top left), and a zoomed-in subarea (white rectangle) showing digital aerial photogrammetry (DAP)-based canopy height models (CHMs) calculated based on point clouds with 234 p/m^2 (top right), 59 p/m^2 (bottom left), and 15 p/m^2 (bottom right).

Ronneberger et al. (2015), which is well suited for image segmentation tasks and has been effectively used in forest-related studies (Freudenberg et al., 2022; Schiefer et al., 2020; Wagner et al., 2019). It is characterized by its encoder-decoder structure. The encoder part consists of several convolutional layers, which extract features from the input images, followed by pooling operations that reduce spatial information while preserving essential features. In the decoder part, spatial information is progressively restored with upsampling operations (Kattenborn et al., 2021). Skip connections between corresponding encoder and decoder layers ensure that the model can use relevant features extracted earlier to improve final output, making it a fully convolutional network (Long et al., 2015).

We used a ResNet34 (He et al., 2016) as backbone, pre-trained on ImageNet. To adapt the backbone to our input of five channels (RGB, NIR, and DAP-based CHM heights), we added an extra convolution layer to convert these five channels into a three-channel format compatible with ResNet34 (Iakubovskii, 2019). This enabled compatibility with the pre-trained weights while preserving the additional input information. The model architecture is illustrated in Fig. 4. We applied a sigmoid activation function to obtain model predictions as probabilities for each pixel between 0 and 1. The Adam optimizer (Kingma and Ba, 2014), initialized with a learning rate of 0.001, was used for stochastic gradient descent. We used binary cross-entropy (BCE) as loss function, which is widely used for binary semantic segmentation tasks, such as, in our case, distinguishing gaps from non-gaps. BCE calculates the difference between the predicted output and the true binary mask as follows:

$$BCE = -\frac{1}{N}\sum_{i=1}^{N} y_i \, log(p(y_i)) + (1-y_i) \, log(1-p(y_i)) \tag{1}$$

Where y is the label of the true binary mask, $p(y)$ is the predicted probability of pixel i being a canopy gap, and N is the total number of pixels in the image.

The training dataset was split into multiple tiles of size 224 × 224 pixels, which can be handled by the model (Fig. 5). From the complete dataset, 80 % were used for training and 20 % for validation. The split was performed randomly to ensure a diverse representation of canopy gap characteristics in both sets. In order to increase the diversity of the training dataset and to prevent overfitting, data augmentation was

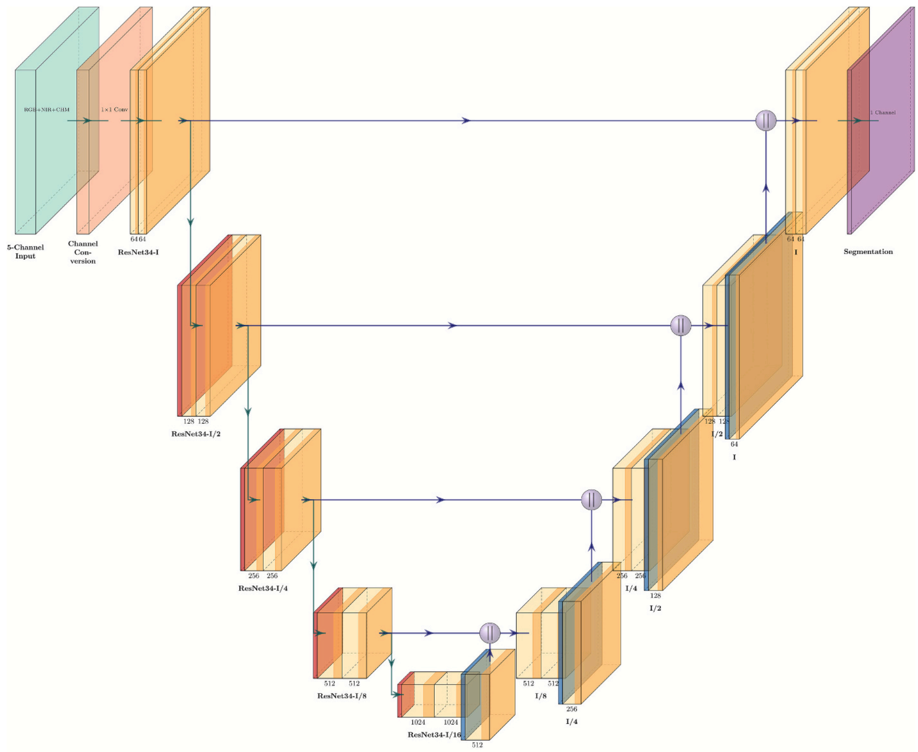

Fig. 4. Simplified U-Net architecture with a ResNet34 backbone. An additional convolution layer was added to adapt the five-channel input (RGB, NIR, DAP-CHM) to the three-channel format required by ResNet34.

applied by rotating the tiles by 90, 180, and 270 degrees. We evaluated the performance of our model after each epoch during the training process by calculating the BCE loss, the intersection over union (IoU), and the F1-score for both the training and validation datasets. The metrics are defined as follows:

$$IoU = \frac{TP}{TP + FN + FP} \quad (2)$$

$$precision = \frac{TP}{TP + FP} \quad (3)$$

$$recall = \frac{TP}{TP + FN} \quad (4)$$

$$F1 - score = 2 \times \frac{precision \times recall}{precision + recall} \quad (5)$$

Where TP are the true positives, FP are the false positives, and FN are the false negatives.

The maximum number of epochs was set to 100. However, the implementation of an early stopping ensured that training was stopped if the validation F1-score did not improve for 10 epochs. Additionally, the learning rate was reduced after 5 epochs of no improvement in the validation F1-score. The whole model workflow was written in Python 3.10.12 and is mainly based on the Segmentation Models library (Iakubovskii, 2019). We trained the model on a computer equipped with an AMD Ryzen Threadripper PRO 5975WX processor (3600 MHz, 32 cores) and 256 GB internal memory.

2.6. Model application and comparison with DAP-derived canopy gaps

The model was applied to the three test areas of size 1 × 1 km not used during model training. To obtain a binary canopy gap mask, we thresholded the pixel-wise predicted probabilities at 0.3, 0.4, and 0.5, to determine differences in the predicted gaps and their accuracy. We calculated the IoU, precision, recall, and the F1-score to assess prediction accuracy. Additionally, the predicted gap area per test area (in hectare and percent) was calculated to complement these metrics. All metrics and the predicted gap area were computed only within valid prediction extent, as the final predictions cover a smaller area (~0.8 km^2) than the original test tiles (1 km^2) due to the tiling process.

Further, we compared our CNN-predictions of canopy gaps with those obtained using a DAP-based CHM alone. We did this by applying our canopy gap detection method, described in Section 2.3, to the DAP-based CHMs of the three test areas (only highest CHM quality). IoU, precision, recall, and F1-score were calculated again using ALS-derived canopy gaps as reference. The total number of canopy gaps as well as the number of canopy gaps ≤50 m^2, which we considered small gaps, were obtained for all three mapping outcomes (ALS-based, DAP-based, CNN-prediction).

3. Results

3.1. Model training

Model training was stopped after 19 epochs, as the F1-score for the validation dataset reached its highest value of 0.64 and did not improve during the following 10 epochs. Similarly, the validation IoU reached a value of 0.48 after epoch 19 and did not improve in subsequent epochs. The BCE validation loss reached 0.14 at epoch 19 and decreased only slightly to 0.13 at epoch 25. However, we defined the best model based on the validation F1-score. Hence, the model trained for 19 epochs was selected for further application to unseen test areas.

3.2. Prediction of canopy gaps on unseen test areas

Fig. 6 shows the three test areas and the corresponding predictions of canopy gaps. As an example, smaller subareas from one of the test areas are visualized in Fig. 7. From a visual perspective, the predictions of

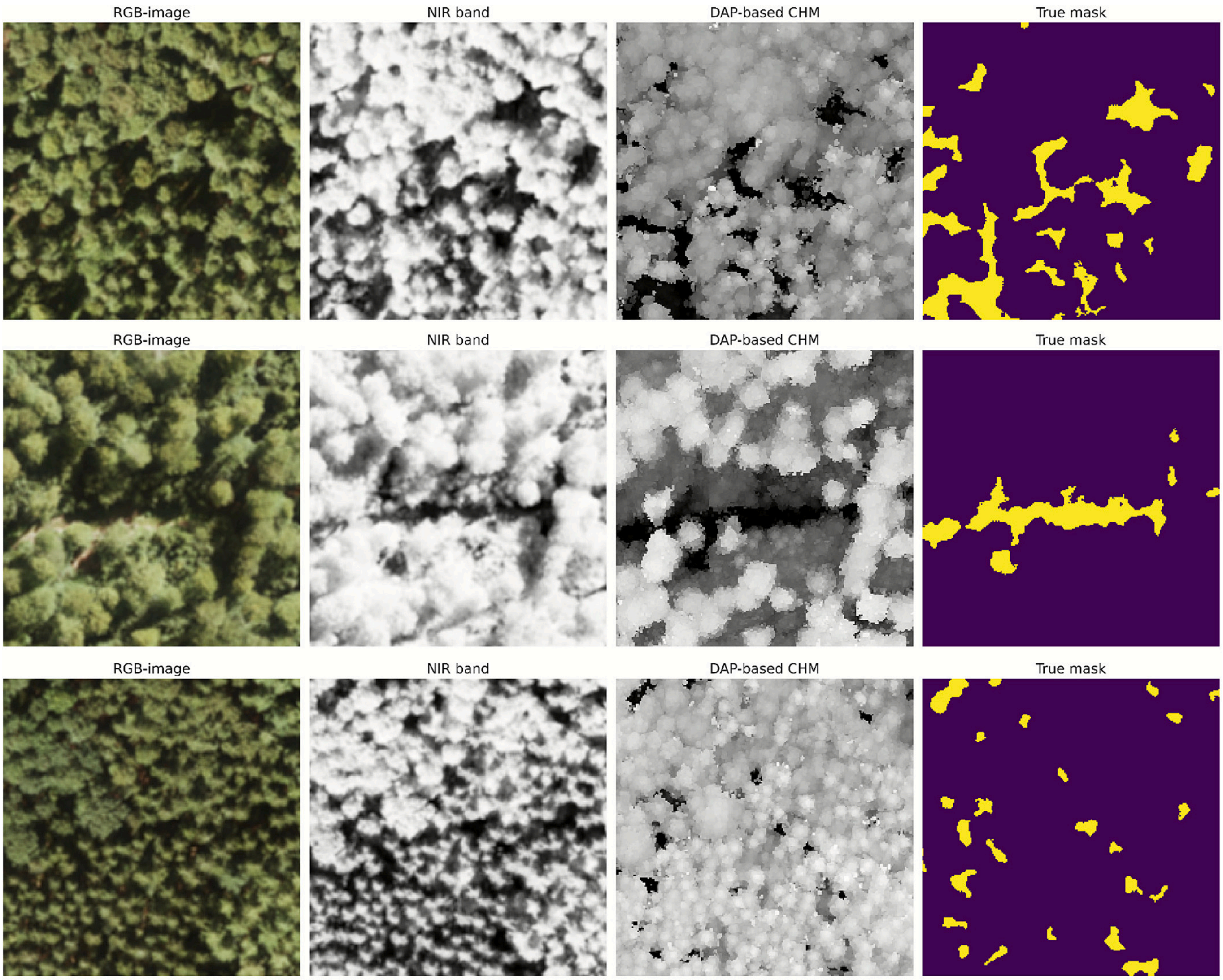

Fig. 5. Example 224 × 224 pixel tiles showing the channels used for model training. For illustrative purposes, the red, green, and blue channels are shown as one RGB true color image. (For interpretation of the references to color in this figure legend, the reader is referred to the web version of this article.)

canopy gaps align well with the ALS-based true mask. However, some larger openings detected in the ALS-based CHMs are either missing or appear disconnected in the predictions, especially in test area 3. In the zoomed-in subareas (Fig. 7), particularly the one in the center, it is clearly visible that smaller canopy gaps, which are absent in the corresponding DAP-based CHM but distinct in their spectral characteristics from the surrounding trees, were predicted accurately.

To assess the impact of CHM quality, we evaluated model performance across three pyramid levels (2, 1, and 0) used in the image-matching process, which resulted in different point densities and canopy surface representations. These are referred to as CHM quality levels. The corresponding evaluation metrics per test area and DAP-based CHM quality level are shown in Table 3. The IoU varied only slightly between the quality levels for each area. Similarly, the F1-score showed minor differences across the quality levels, balancing fluctuations in precision and recall. The largest differences in the F1-score between quality levels were observed for test area 3, where both recall and precision varied the most. Precision was higher than recall across all quality levels in test areas 1 and 3, whereas recall exceeded precision in test area 2. Overall, the model performed best on test area 2 (mean IoU $\approx$ 0.77, mean F1-score $\approx$ 0.74), while it performed worst on test area 3 (mean IoU $\approx$ 0.69, mean F1-score $\approx$ 0.60). Considering the predicted gap area, a slight overestimation of canopy gaps was observed for test area 2, whereas in test areas 1 and 3, the predicted gap area was below the true gap area. In test area 1, the predicted gap area closely matched the true gap area, particularly for CHM quality levels 0 and 1. A general decrease in the predicted gap area was noticed across all test areas for CHM quality level 2 (lowest point density).

The metrics as well as the predicted gap area were based on a threshold of 0.5 for prediction probabilities, as it provided the best results for test areas 1 and 2. Although a lower threshold (0.3) resulted in marginally better performance for test area 3, we prioritized consistency and comparability across all test areas and thus selected the threshold that performed best overall.

3.3. Comparison with DAP-derived canopy gaps

ALS- and DAP-based CHMs for all three test areas, along with their corresponding canopy gap raster masks, are provided in the Supplementary Data (Fig. S1). Table 4 presents IoU, precision, recall, and F1-scores for the DAP-derived canopy gaps compared to those obtained from ALS (the reference). IoU and F1-score were lower when using a DAP-based CHM alone for canopy gap detection compared to the model predictions. However, this difference was not equally pronounced across all three test areas. While the metrics differed only slightly for test area 2, the differences were more substantial for test areas 1 and 3. This is

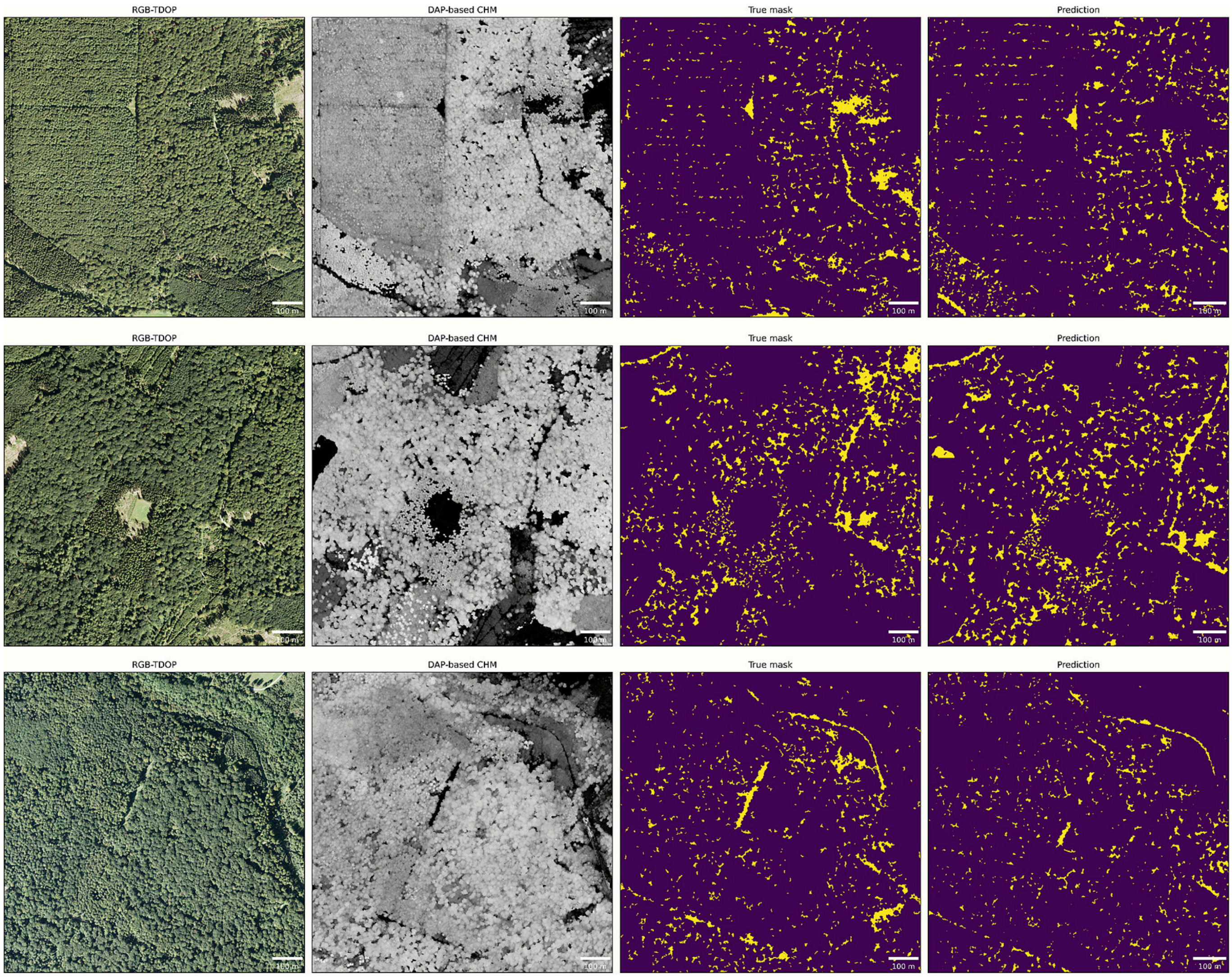

Fig. 6. Predictions of canopy gaps for test area 1 (top), area 2 (center), and area 3 (bottom): Each row includes the RGB true digital orthophoto (RGB-TDOP), the digital aerial photogrammetry (DAP)-based canopy height model (CHM) (level 0), the true mask showing the reference canopy gaps derived from airborne laser scanning (ALS)-based CHMs, and the predicted canopy gaps obtained by the model.

also evident in the canopy gap raster masks (see Supplementary Data, Fig. S1), where several gaps are missing in the DAP-based mask for both test areas compared to the ALS-based mask, also reflected by the low recall values (0.46/0.37). On average, the model improved the F1-score by 0.08 compared to using DAP-based CHMs alone. Visually, this is particularly noticeable for smaller canopy gaps detected in ALS-based CHMs, which are often absent in DAP-based CHMs. The distribution of gap sizes, separated by the different sources (ALS, DAP, prediction), also shows this lower proportion of smaller canopy gaps in the DAP-based CHMs (Fig. 8). This trend of missing gaps is particularly evident up to a gap size of approximately 50 m^2, while the distribution of such smaller gaps in the predictions more closely aligns with that of the ALS-based gaps. Table 5 shows that relative proportions of small canopy gaps ($\leq$ 50 m^2) are lower in DAP-based CHMs compared to ALS-based detection, whereas the model predictions show higher proportions relative to ALS-based canopy gaps. While these proportions offer insights into the general representation of small gaps, they do not reflect spatial agreement with ALS-based gaps.

4. Discussion

4.1. Segmentation performance and influencing factors

ALS is a highly effective technology for detecting and tracking canopy gaps. Several studies demonstrated its suitability, in particular, for characterizing canopy gaps across large forested areas in different regions of the world (Goodbody et al., 2020; Gorgens et al., 2023; Hagemann et al., 2022). DAP, as an alternative to ALS for canopy gap detection, has shown lower performance, particularly in detecting small canopy openings in old seral stage forests (Dietmaier et al., 2019; White et al., 2018). To address these limitations, we developed a cross-technological approach in which a CNN was trained to predict canopy gaps based on height information from DAP-based CHMs and spectral information from TDOPs. ALS-derived canopy gaps served as reference.

The resulting segmentation maps of canopy gaps and non-canopy gaps for our three test areas revealed slightly different performance of the CNN, as confirmed by the calculated error metrics. Overall, IoU (0.67–0.77) and F1-score (0.56–0.74) showed moderate to small variation across the test areas. While segmentation performance was comparable for test areas 1 and 2, it was lower in test area 3. The quality level of the DAP-based point clouds used for CHM calculation appears to

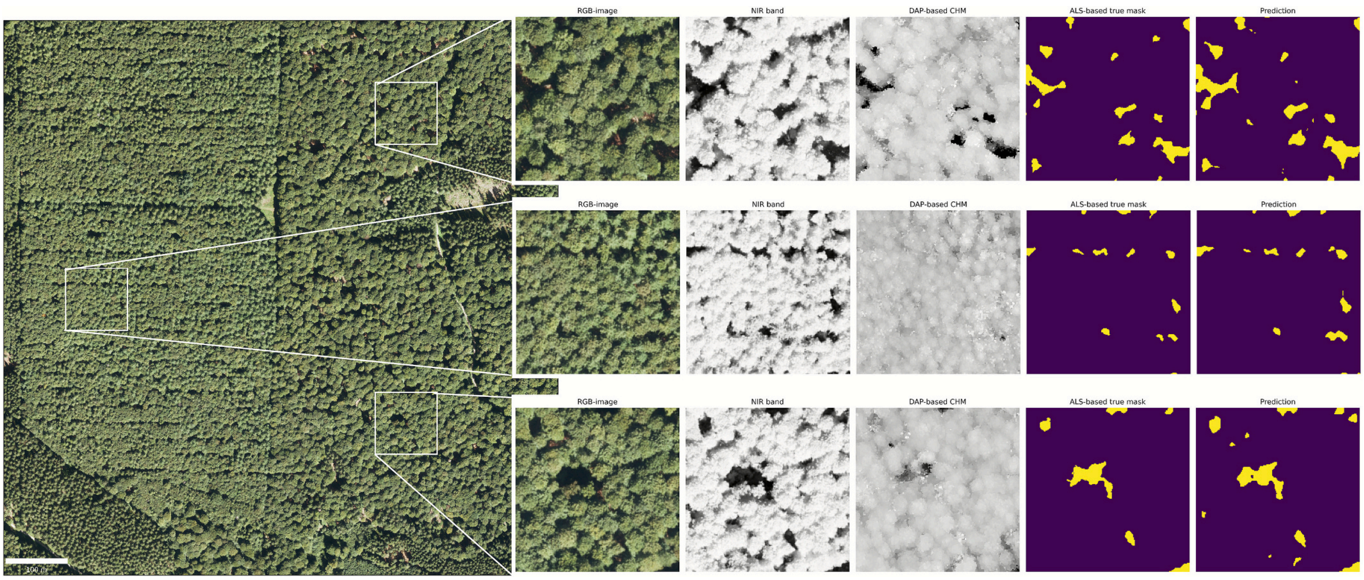

Fig. 7. Test area 1 and three enlarged subareas (white rectangles) representing different types of canopy gap situations: Several larger gaps (top), several smaller gaps (center), and a mix of both (bottom).

Table 3
Intersection over union (IoU), precision, recall, F1-score, and predicted gap area per quality level of digital aerial photogrammetry (DAP)-based canopy height models (CHMs) for prediction on test area 1 (true gap area ≈ 4.8 ha, 6 %), test area 2 (true gap area ≈ 6.8 ha, 8.5 %), and test area 3 (true gap area ≈ 4.4 ha, 5.4 %).

Pyramid level of DAP-based point cloud used for CHM calculation (point density)	IoU	Precision	Recall	F1-score	Predicted gap area (ha / %)
Test area 1					
Level 0 (234 p/m^2)	0.76	0.73	0.70	0.71	4.6 / 5.8
Level 1 (59 p/m^2)	0.76	0.74	0.70	0.72	4.6 / 5.8
Level 2 (15 p/m^2)	0.76	0.78	0.65	0.71	4.1 / 5
Test area 2					
Level 0 (275 p/m^2)	0.76	0.69	0.77	0.73	7.6 / 9.4
Level 1 (69 p/m^2)	0.77	0.69	0.79	0.74	7.8 / 9.7
Level 2 (17 p/m^2)	0.77	0.71	0.77	0.74	7.3 / 9.2
Test area 3					
Level 0 (180 p/m^2)	0.70	0.74	0.53	0.61	3.1 / 3.9
Level 1 (45 p/m^2)	0.71	0.74	0.54	0.63	3.2 / 4
Level 2 (11 p/m^2)	0.67	0.80	0.43	0.56	2.3 / 2.9

Table 4
Intersection over union (IoU), precision, recall, and F1-score comparing canopy gaps obtained by digital aerial photogrammetry (DAP)-based canopy height models (CHMs) with Airborne Laser Scanning (ALS)-based canopy gaps for the three test areas.

	IoU	Precision	Recall	F1-score
Test area 1	0.69	0.84	0.46	0.59
Test area 2	0.74	0.86	0.58	0.69
Test area 3	0.66	0.91	0.37	0.53

have a minor impact on segmentation results (IoU variation: ± 0.02, F1-score variation: ± 0.04), whereas the variation observed among the three test areas was considerably larger (IoU variation: ± 0.05, F1-score variation: ± 0.09). This suggests that factors related to test area, such as forest structure, may have a stronger influence on segmentation performance. We observed a higher number of larger canopy openings in test area 3 in comparison to the other two test areas, many of which were not, or only partially, predicted by the model. One possible explanation is misleading spectral information, as these larger gaps tend to appear brighter with fewer shadows than smaller canopy gaps. This may have contributed to the lower segmentation performance in test area 3, as these large gaps account for a substantial share of the total gap area. However, since test area 3 also exhibited the lowest point densities across all pyramid levels, indicates that DAP-CHM quality still plays a role in canopy gap segmentation by the model, particularly when point densities are relatively low (pyramid level 2). The impact of DAP-CHM quality on canopy gap detection was also observed by Zielewska-Büttner et al. (2016b), who reported a higher number of pixels with missing information due to higher pyramid level during image-matching. Such pixels are assigned new values via interpolation, which results in smoother DAP-CHMs, ultimately reducing gap detection accuracy.

We deduce that the CNN was generally less prone to predict false gaps (false positives) but more likely to miss actual gaps (false negatives), particularly in test areas 1 and 3, as indicated by the precision and recall values and the fact that the predicted gap area was smaller than the true gap area in these two areas. This issue is not primarily due to undetected small gaps, but rather due to incomplete or entirely missing predictions of larger canopy openings by the model.

4.2. Comparison of DAP-based with predicted canopy gaps

The comparison between the predicted and DAP-derived canopy gaps demonstrated better performance of the model predictions. As indicated by the error metrics, differences between the predicted and DAP-derived canopy gaps were particularly distinct for test area 3, suggesting that our approach might be beneficial for lower quality DAP-CHMs. However, substantial differences in IoU and F1-score were also observed for test area 1, despite its relatively high quality DAP-CHM. The forest structure, including the prevalence of small canopy gaps, may also influence detection accuracy. Test area 1 has a slightly higher proportion of smaller gaps (≤ 50 m^2) compared to test area 2 and 3. Smaller gaps are more challenging to detect in DAP-based CHMs (White et al., 2018), which likely contributes to the larger difference in IoU and F1-score between the predicted and DAP-derived canopy gaps in test area 1. In contrast, test area 2, which had the lowest proportion of small gaps relative to the total number of gaps, showed the smallest difference in these metrics.

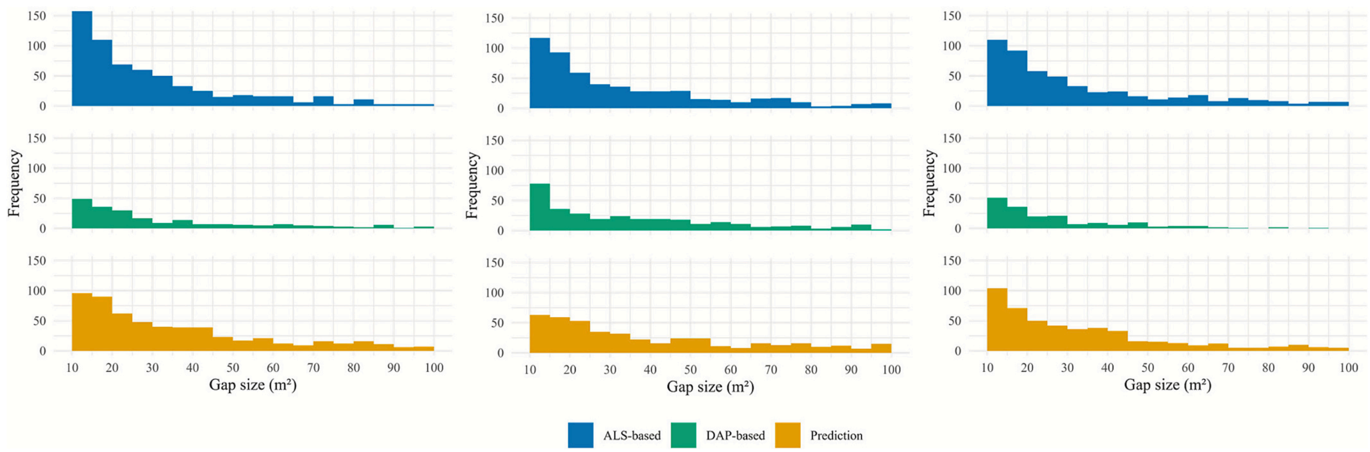

Fig. 8. Histograms of gap sizes (10–100 m^2) for test area 1 (left), area 2 (center), and area 3 (right). Canopy gaps were obtained from airborne laser scanning (ALS)-based, digital aerial photogrammetry (DAP)-based canopy height models (CHMs), and from the prediction.

Table 5
Total number of canopy gaps and number of canopy gaps ≤50 m^2 for the three test areas, along with the relative proportions of digital aerial photogrammetry (DAP)-based and predicted canopy gaps compared to airborne laser scanning (ALS)-based detection.

	Total canopy gaps	Canopy gaps ≤ 50 m^2	Proportion of total canopy gaps rel. to ALS	Proportion of canopy gaps ≤ 50 m^2 rel. to ALS
Test area 1				
ALS-based	707	525		
DAP-based	251	169	36 %	32 %
Prediction	662	437	94 %	83 %
Test area 2				
ALS-based	687	430		
DAP-based	412	241	60 %	56 %
Prediction	623	304	91 %	71 %
Test area 3				
ALS-based	578	405		
DAP-based	206	160	36 %	40 %
Prediction	542	390	94 %	96 %

Studies frequently identified shadow occurrence as a major error source in DAP-based canopy gap detection (Dietmaier et al., 2019; White et al., 2018; Zielewska-Büttner et al., 2016a), which likely contributed to the lower detection rate in our DAP-derived CHMs. However, our model may leverage these shadows by utilizing their specific reflective properties (Liu et al., 2024) to distinguish between darker gaps and the brighter surrounding canopy. Consequently, the advantage of our model over DAP-based gap detection is particularly evident in forest areas with a high prevalence of smaller gaps. DAP-derived gaps could be used to complement the model predictions for larger canopy openings, as these are less challenging to detect in DAP-based CHMs, whereas the model showed limitations in accurately capturing them.

4.3. Methodological considerations of deep learning for canopy gap detection

As this study is among the first of its kind, direct comparisons with other studies are challenging. Additionally, technical factors such as variations in CNN architectures, as well as environmental differences in the investigated forest areas, complicate comparisons. The most comparable study is that of Htun et al. (2024), who also applied a deep learning approach to detect canopy gaps. However, unlike our study, they used UAV imagery and derived CHMs. They tested different models in an uneven-aged mixed forest in northern Japan and achieved the most robust segmentation results with a U-Net using ResNet101 as backbone pre-trained on ImageNet. IoU was 0.62/0.66 and F1-score 0.77/0.79, depending on the area.

Another study involving deep learning in the context of canopy gap detection is that of Lassalle and de Souza Filho (2022). They used very-high-resolution satellite imagery to map gaps in mangrove forests and simultaneously assess their recovery stage using a Mask R-CNN, a framework for instance segmentation (He et al., 2017). Their model achieved an overall accuracy of 98,9 % in distinguishing gap and non-gap areas. However, the gap areas in their reference dataset covered a smaller range, from 27.3 to 861.9 m^2, and the general shape of mangrove gaps is similar, explaining this high accuracy (Lassalle and de Souza Filho, 2022). A direct comparison of the metrics achieved by our study is not appropriate, as the methods differ in several aspects, such as the approach for reference data generation (manual delineation vs. automatic detection) and the source of remote sensing data (UAV/satellite vs. airborne). While the best performing model in Htun et al. (2024) utilized only RGB spectral information, they also applied the same model architecture incorporating both DAP-CHM and RGB data without pre-training. This model showed slightly lower performance (IoU: 0.54/0.56, F1-score: 0.70/0.72). However, in the case of non-pre-trained models, they highlighted that integrating height and spectral information improves model performance, leading to their suggestion to pre-train such multi-source models on large multi-channel datasets.

A key limitation in applying transfer learning to remote sensing data is that widely used backbones are typically trained on standard RGB imagery like in the ImageNet dataset, whereas remote sensing data often contain additional information (Kattenborn et al., 2021). This presents a potential limitation for our model, as we also pre-trained it on ImageNet despite incorporating NIR as an additional spectral band and CHM height information. Several remote sensing studies on vegetation analyses utilizing deep learning have pointed to this issue, highlighting the need for pre-trained models capable of handling multi-channel data (Ecke et al., 2024; Htun et al., 2024). One key aspect of multi-channel data in forest applications could be the inclusion of height information, which has been explored for tree and plant species identification with CNNs. However, these studies have shown only minor (Schiefer et al., 2020) to none or unclear (Ecke et al., 2024; Kattenborn et al., 2020) improvements in model performance when adding CHM height information to spectral bands, most likely because structural information such as canopy height is already captured in the imagery through patterns of shading and lighting variation (Kattenborn et al., 2020). In contrast, in our study, we assume that using only spectral data would not be beneficial, as the presence or absence of canopy gaps is directly linked to the height.

To advance deep learning applications in forestry remote sensing, models should not only be pre-trained with spectral imagery, but also incorporate height information from laser scanning or DAP-derived CHMs, which is often missing in existing datasets (see Table 1 in Schmitt et al., 2019). Expanding pre-training to include height data could greatly benefit a variety of forest applications related to forest's spatial structure and may be particularly relevant for LiDAR data fusion (Balestra et al., 2024).

4.4. Potential of ALS for reference data generation

ALS offers significant potential for generating reference data. CNNs require large amounts of labeled data, and a common approach is to use remote sensing products for visual interpretation and subsequent annotation of the desired class(es) (Kattenborn et al., 2021). However, this process is highly labor-intensive and often becomes a bottleneck, particularly in complex environments such as forest ecosystems (Borowiec et al., 2022). Automatically-derived reference data can help overcome this challenge. In our study, we achieved this by automatically detecting canopy gaps in ALS-based CHMs, resulting in over 15,000 gap polygons for training our model.

A similar approach was applied by Weinstein et al. (2019) for individual tree detection. They used LiDAR data to automatically generate labeled tree crowns as bounding boxes, which were then combined with manually annotated labels to train a CNN. Incorporating a small number of manually delineated canopy gaps alongside automatically generated reference gaps could be a useful addition to further refine our approach.

While ALS enables large-scale and objective reference data generation, the implemented gap definition directly influences what the model learns. Parameters such as gap size and height thresholds can vary significantly among definitions, as described in Section 2.3, meaning that segmentation outputs could differ depending on the gap definition applied for reference data generation. Additionally, technical factors such as point density, CHM resolution, and the algorithm chosen for CHM calculation influence gap detection (Fischer et al., 2024) and, consequently, the segmentation by the model. In this study, we used high-resolution ALS data with sufficient point density for forest structure assessment. Nonetheless, we acknowledge that ALS-derived gaps may still contain errors or systematic biases, particularly in areas with dense vegetation or complex terrain.

5. Conclusion

While numerous studies have demonstrated that ALS is a highly effective technology for detecting canopy gaps, it is still a fact that ALS data availability remains limited, whereas DAP data is more frequently accessible. This study was designed as a baseline to address the technical limitations of DAP for canopy gap detection. We applied a cross-technological approach involving ALS data to automatically generate reference gap polygons, which were then used to train a CNN with spectral (RGBI) and height (DAP-based CHM) information as input data.

Our results demonstrated the feasibility of detecting canopy gaps in the absence of ALS data. Once trained on ALS-based reference gaps, our model can be applied using only image-derived inputs. Compared to using DAP-based CHMs alone for canopy gap detection, the model achieved improved segmentation results, which represents a significant advancement in particular for detecting small canopy gaps in mature and old-growth forest stands. However, the benefit of our approach depends not only on technical factors such as DAP-CHM quality, but also on environmental conditions like forest structure. While smaller canopy gaps were often predicted accurately, the model exhibited difficulties in fully detecting larger canopy openings, likely due to misleading spectral information in bright, few shadow areas. This issue could be addressed by incorporating DAP-derived gaps above a certain area threshold, as larger gaps are generally easier to detect in DAP-based CHMs. The influence of DAP-CHM quality, primarily influenced by point density after image-matching, on segmentation performance was somewhat ambiguous, although we observed a trend toward reduced accuracy when using CHMs derived from DAP-based point clouds with pyramid level 2. While this demonstrates some robustness to quality variations, adequate image acquisition quality remains a prerequisite for reliable gap detection.

The detection of canopy gaps from only image-derived inputs offers promising applications for ecological and forestry practices in regions where ALS data availability is limited. It enables temporal analyses over longer time periods, which can support forest management and biodiversity monitoring. Specifically, automated gap detection can facilitate monitoring of forest structural complexity and the assessment of natural regeneration processes.

The overall performance of our model could be further enhanced if pre-trained model architectures incorporating height information were available. Additionally, exploring alternative CNN architectures may offer further potential to improve segmentation results. Future research should focus on testing the model's transferability to other regions with entirely different forest structures and acquisition settings, including images captured at different points in time. Nevertheless, the presented approach provides a valuable improvement over using DAP-based CHMs alone for canopy gap detection.

CRediT authorship contribution statement

Florian Franz: Writing – original draft, Visualization, Software, Methodology, Formal analysis, Data curation, Conceptualization. **Dominik Seidel:** Writing – original draft, Visualization, Software, Methodology, Formal analysis, Data curation, Conceptualization. **Philip Beckschäfer:** Writing – original draft, Visualization, Software, Methodology, Formal analysis, Data curation, Conceptualization.

Declaration of generative AI and AI-assisted technologies in the writing process

During the preparation of this work the author(s) used [ChatGPT] to adjust the order of sentences for coherence. After using this tool/service, the author(s) reviewed and edited the content as needed and take(s) full responsibility for the content of the published article.

Funding

This work was supported by the German Federal Ministry of Agriculture, Food and Regional Identity (BMLEH) administrated by the Agency for Renewable Resources (FNR) [grant number 2220NR102X].

Declaration of competing interest

The authors declare that they have no known competing financial interests or personal relationships that could have appeared to influence the work reported in this paper.

Acknowledgements

The authors would like to express their gratitude to the state forest enterprise of Lower Saxony for providing airborne laser scanning and imagery data. Additionally, we acknowledge Kirsten Krüger for helpful discussions on canopy gap detection methods. We also thank Georgia Reeves for her careful proofreading of the manuscript and valuable suggestions regarding grammar, spelling, and overall language clarity.

Appendix A. Supplementary data

Supplementary data to this article can be found online at https://doi.

org/10.1016/j.ecoinf.2025.103558.

Data availability

The code used in this study is available at https://github.com/FloFranz/canopy-gap-detection.

Data are available at https://zenodo.org/records/17829462.

References

Asner, G.P., Kellner, J.R., Kennedy-Bowdoin, T., Knapp, D.E., Anderson, C., Martin, R.E., 2013. Forest canopy gap distributions in the southern Peruvian Amazon. PLoS One 8 (4), e60875. https://doi.org/10.1371/journal.pone.0060875.

Bagnato, S., Marziliano, P.A., Sidari, M., Mallamaci, C., Marra, F., Muscolo, A., 2021. Effects of gap size and cardinal directions on natural regeneration, growth dynamics of trees outside the gaps and soil properties in European beech forests of southern Italy. Forests 12 (11), 1563. https://doi.org/10.3390/f12111563.

Balestra, M., Marselis, S., Sankey, T.T., Cabo, C., Liang, X., Mokroš, M., Peng, X., Singh, A., Stereńczak, K., Vega, C., Vincent, G., Hollaus, M., 2024. LiDAR data fusion to improve forest attribute estimates: a review. Curr. For. Rep. 10 (4), 281–297. https://doi.org/10.1007/s40725-024-00223-7.

Borowiec, M.L., Dikow, R.B., Frandsen, P.B., McKeeken, A., Valentini, G., White, A.E., 2022. Deep learning as a tool for ecology and evolution. Methods Ecol. Evol. 13 (8), 1640–1660. https://doi.org/10.1111/2041-210X.13901.

Chen, J., Wang, L., Jucker, T., Da, H., Zhang, Z., Hu, J., Yang, Q., Wang, X., Qin, Y., Shen, G., Shu, L., Zhang, J., 2023. Detecting forest canopy gaps using unoccupied aerial vehicle RGB imagery in a species–rich subtropical forest. Remote Sens. Ecol. Conserv. 9 (5), 671–686. https://doi.org/10.1002/rse2.336.

Chung, C.-H., Wang, J., Deng, S.-L., Huang, C., 2022. Analysis of canopy gaps of coastal broadleaf Forest plantations in Northeast Taiwan using UAV lidar and the Weibull distribution. Remote Sens. 14 (3), 667. https://doi.org/10.3390/rs14030667.

Dalagnol, R., Phillips, O.L., Gloor, E., Galvão, L.S., Wagner, F.H., Locks, C.J., Aragão, L.E.O.C., 2019. Quantifying canopy tree loss and gap recovery in tropical forests under low-intensity logging using VHR satellite imagery and airborne LiDAR. Remote Sens. 11 (7), 817. https://doi.org/10.3390/rs11070817.

Dalagnol, R., Wagner, F.H., Galvão, L.S., Streher, A.S., Phillips, O.L., Gloor, E., Pugh, T.A.M., Ometto, Jean P.H.B., Aragão, L.E.O.C., 2021. Large-scale variations in the dynamics of Amazon forest canopy gaps from airborne lidar data and opportunities for tree mortality estimates. Sci. Rep. 11 (1), 1388. https://doi.org/10.1038/s41598-020-80809-w.

de Freitas, C.R., Enright, N.J., 1995. Microclimatic differences between and within canopy gaps in a temperate rainforest. Int. J. Biometeorol. 38 (4), 188–193. https://doi.org/10.1007/BF01245387.

Denslow, J.S., 1980. Gap partitioning among tropical rainforest trees. Biotropica 12 (2), 47–55. https://doi.org/10.2307/2388156.

Dietmaier, A., McDermid, G.J., Rahman, M.M., Linke, J., Ludwig, R., 2019. Comparison of LiDAR and digital aerial photogrammetry for characterizing canopy openings in the boreal Forest of northern Alberta. Remote Sens. 11 (16), 1919. https://doi.org/10.3390/rs11161919.

Drößler, L., von Lüpke, B., 2005. Canopy gaps in two virgin beech forest reserves in Slovakia. J. For. Sci. 51 (10), 446–457. https://doi.org/10.17221/4578-JFS.

Ecke, S., Stehr, F., Frey, J., Tiede, D., Dempewolf, J., Klemmt, H.-J., Endres, E., Seifert, T., 2024. Towards operational UAV-based forest health monitoring: species identification and crown condition assessment by means of deep learning. Comput. Electron. Agric. 219, 108785. https://doi.org/10.1016/j.compag.2024.108785.

Eckerter, T., Buse, J., Bauhus, J., Förschler, M.I., Klein, A.M., 2021. Wild bees benefit from structural complexity enhancement in a forest restoration experiment. For. Ecol. Manag. 496, 119412. https://doi.org/10.1016/j.foreco.2021.119412.

FAO, 2020. Global Forest Resources Assessment 2020: Main Report. https://doi.org/10.4060/ca9825en.

Feldmann, E., Drößler, L., Hauck, M., Kucbel, S., Pichler, V., Leuschner, C., 2018. Canopy gap dynamics and tree understory release in a virgin beech forest, Slovakian Carpathians. For. Ecol. Manag. 415–416, 38–46. https://doi.org/10.1016/j.foreco.2018.02.022.

Fischer, F.J., Jackson, T., Vincent, G., Jucker, T., 2024. Robust characterisation of forest structure from airborne laser scanning—a systematic assessment and sample workflow for ecologists. Methods Ecol. Evol. 15 (10), 1873–1888. https://doi.org/10.1111/2041-210X.14416.

Freudenberg, M., Magdon, P., Nölke, N., 2022. Individual tree crown delineation in high-resolution remote sensing images based on U-Net. Neural Comput. & Applic. 34 (24), 22197–22207. https://doi.org/10.1007/s00521-022-07640-4.

Garbarino, M., Borgogno Mondino, E., Lingua, E., Nagel, T.A., Dukić, V., Govedar, Z., Motta, R., 2012. Gap disturbances and regeneration patterns in a Bosnian old-growth forest: a multispectral remote sensing and ground-based approach. Ann. For. Sci. 69 (5), 617–625. https://doi.org/10.1007/s13595-011-0177-9.

Getzin, S., Nuske, R., Wiegand, K., 2014. Using unmanned aerial vehicles (UAV) to quantify spatial gap patterns in forests. Remote Sens. 6 (8), 6988–7004. https://doi.org/10.3390/rs6086988.

Goodbody, T.R.H., Coops, N.C., White, J.C., 2019. Digital aerial photogrammetry for updating area-based Forest inventories: a review of opportunities, challenges, and future directions. Curr. For. Rep. 5 (2), 55–75. https://doi.org/10.1007/s40725-019-00087-2.

Goodbody, T.R.H., Tompalski, P., Coops, N.C., White, J.C., Wulder, M.A., Sanelli, M., 2020. Uncovering spatial and ecological variability in gap size frequency distributions in the Canadian boreal forest. Sci. Rep. 10 (1), 6069. https://doi.org/10.1038/s41598-020-62878-z.

Gorgens, E.B., Keller, M., Jackson, T., Marra, D.M., Reis, C.R., de Almeida, D.R.A., Coomes, D., Ometto, J.P., 2023. Out of steady state: tracking canopy gap dynamics across Brazilian Amazon. Biotropica 55 (4), 755–766. https://doi.org/10.1111/btp.13226.

Gustafsson, L., Bauhus, J., Asbeck, T., Augustynczik, A.L.D., Basile, M., Frey, J., Gutzat, F., Hanewinkel, M., Helbach, J., Jonker, M., Knuff, A., Messier, C., Penner, J., Pyttel, P., Reif, A., Storch, F., Winiger, N., Winkel, G., Yousefpour, R., Storch, I., 2020. Retention as an integrated biodiversity conservation approach for continuous-cover forestry in Europe. Ambio 49 (1), 85–97. https://doi.org/10.1007/s13280-019-01190-1.

Hagemann, N., Magdon, P., Schnell, S., Pommerening, A., 2022. Analysing gap dynamics in forest canopies with landscape metrics based on multi-temporal airborne laser scanning surveys – a pilot study. Ecol. Indic. 145, 109627. https://doi.org/10.1016/j.ecolind.2022.109627.

He, K., Zhang, X., Ren, S., Sun, J., 2016. Deep residual learning for image recognition. In: 2016 IEEE Conference on Computer Vision and Pattern Recognition (CVPR), pp. 770–778. https://doi.org/10.1109/CVPR.2016.90.

He, K., Gkioxari, G., Dollar, P., Girshick, R., 2017. Mask R-CNN. In: 2017 IEEE International Conference on Computer Vision (ICCV), pp. 2980–2988. https://doi.org/10.1109/ICCV.2017.322.

Heidrich, L., Bae, S., Levick, S., Seibold, S., Weisser, W., Krzystek, P., Magdon, P., Nauss, T., Schall, P., Serebryanyk, A., Wöllauer, S., Ammer, C., Bässler, C., Doerfler, I., Fischer, M., Gossner, M.M., Heurich, M., Hothorn, T., Jung, K., Kreft, H., Schulze, E.-D., Simons, N., Thorn, S., Müller, J., 2020. Heterogeneity-diversity relationships differ between and within trophic levels in temperate forests. Nat. Ecol. Evol. 4 (9), 1204–1212. https://doi.org/10.1038/s41559-020-1245-z.

Hijmans, R.J., 2024. terra: Spatial Data Analysis. https://github.com/rspatial/terra.

Hobi, M.L., Ginzler, C., Commarmot, B., Bugmann, H., 2015. Gap pattern of the largest primeval beech forest of Europe revealed by remote sensing. Ecosphere 6 (5), 1–15. https://doi.org/10.1890/ES14-00390.1.

Horváth, C.V., Kovács, B., Tinya, F., Schadeck Locatelli, J., Németh, C., Crecco, L., Illés, G., Csépányi, P., Ódor, P., 2023. A matter of size and shape: microclimatic changes induced by experimental gap openings in a sessile oak-hornbeam forest. Sci. Total Environ. 873, 162302. https://doi.org/10.1016/j.scitotenv.2023.162302.

Hou, M., Zhang, G., Li, Y., Xie, J., Zang, L., Liu, Q., Chen, D., Sui, M., He, Y., 2024. The effects of canopy gaps on soil nutrient properties: a meta-analysis. Eur. J. For. Res. 143 (3), 861–873. https://doi.org/10.1007/s10342-024-01660-6.

Htun, N.M., Owari, T., Tsuyuki, S., Hiroshima, T., 2024. Detecting canopy gaps in uneven-aged mixed forests through the combined use of unmanned aerial vehicle imagery and deep learning. Drones 8 (9), 484. https://doi.org/10.3390/drones8090484.

Iakubovskii, P., 2019. Segmentation Models. GitHub. https://github.com/qubvel/segmentation_models.

Jucker, T., 2022. Deciphering the fingerprint of disturbance on the three-dimensional structure of the world's forests. New Phytol. 233 (2), 612–617. https://doi.org/10.1111/nph.17729.

Kattenborn, T., Eichel, J., Wiser, S., Burrows, L., Fassnacht, F.E., Schmidtlein, S., 2020. Convolutional neural networks accurately predict cover fractions of plant species and communities in unmanned aerial vehicle imagery. Remote Sens. Ecol. Conserv. 6 (4), 472–486. https://doi.org/10.1002/rse2.146.

Kattenborn, T., Leitloff, J., Schiefer, F., Hinz, S., 2021. Review on convolutional neural networks (CNN) in vegetation remote sensing. ISPRS J. Photogramm. Remote Sens. 173, 24–49. https://doi.org/10.1016/j.isprsjprs.2020.12.010.

Kern, C.C., Montgomery, R.A., Reich, P.B., Strong, T.F., 2013. Canopy gap size influences niche partitioning of the ground-layer plant community in a northern temperate forest. J. Plant Ecol. 6 (1), 101–112. https://doi.org/10.1093/jpe/rts016.

Kingma, D.P., Ba, J., 2014. Adam: A Method for Stochastic Optimization.

Krüger, K., Senf, C., Jucker, T., Pflugmacher, D., Seidl, R., 2024. Gap expansion is the dominant driver of canopy openings in a temperate mountain forest landscape. J. Ecol. https://doi.org/10.1111/1365-2745.14320.

Kuuluvainen, T., Angelstam, P., Frelich, L., Jõgiste, K., Koivula, M., Kubota, Y., Lafleur, B., Macdonald, E., 2021. Natural disturbance-based forest management: moving beyond retention and continuous-cover forestry. Front. For. Glob. Change 4, 629020. https://doi.org/10.3389/ffgc.2021.629020.

Lassalle, G., de Souza Filho, C.R., 2022. Tracking canopy gaps in mangroves remotely using deep learning. Remote Sens. Ecol. Conserv. 8 (6), 890–903. https://doi.org/10.1002/rse2.289.

Liu, J., Wang, X., Guo, M., Feng, R., Wang, Y., 2024. Shadow detection in remote sensing images based on spectral radiance separability enhancement. IEEE Trans. Pattern Anal. Mach. Intell. 46 (5), 3438–3449. https://doi.org/10.1109/TPAMI.2023.3343728.

Long, J., Shelhamer, E., Darrell, T., 2015. Fully convolutional networks for semantic segmentation. In: 2015 IEEE Conference on Computer Vision and Pattern Recognition (CVPR), pp. 3431–3440. https://doi.org/10.1109/CVPR.2015.7298965.

Mason, W.L., Diaci, J., Carvalho, J., Valkonen, S., 2022. Continuous cover forestry in Europe: usage and the knowledge gaps and challenges to wider adoption. Forestry 95 (1), 1–12. https://doi.org/10.1093/forestry/cpab038.

McCarthy, J., 2001. Gap dynamics of forest trees: a review with particular attention to boreal forests. Environ. Rev. 9 (1), 1–59. https://doi.org/10.1139/er-9-1-1.

Muscolo, A., Bagnato, S., Sidari, M., Mercurio, R., 2014. A review of the roles of forest canopy gaps. J. For. Res. 25 (4), 725–736. https://doi.org/10.1007/s11676-014-0521-7.

Nagel, T.A., Svoboda, M., Rugani, T., Diaci, J., 2010. Gap regeneration and replacement patterns in an old-growth Fagus–Abies forest of Bosnia–Herzegovina. Plant Ecol. 208 (2), 307–318. https://doi.org/10.1007/s11258-009-9707-z.

Nyamgeroh, B.B., Groen, T.A., Weir, M.J.C., Dimov, P., Zlatanov, T., 2018. Detection of forest canopy gaps from very high resolution aerial images. Ecol. Indic. 95, 629–636. https://doi.org/10.1016/j.ecolind.2018.08.011.

Pollock, H.S., Jones, T.M., Tarwater, C.E., Nishikawa, E.T., Brawn, J.D., 2020. Rapid colonization and turnover of birds in a tropical forest treefall gap. J. Field Ornithol. 91 (2), 107–117. https://doi.org/10.1111/jofo.12328.

R Core Team, 2024. R: A Language and Environment for Statistical Computing. R Foundation for Statistical Computing. https://www.R-project.org/.

Rapidlasso GmbH, 2021. LAStools - Efficient LiDAR Processing Software. http://rapidlasso.com/LAStools.

Reis, C.R., Jackson, T.D., Gorgens, E.B., Dalagnol, R., Jucker, T., Nunes, M.H., Ometto, J. P., Aragão, L.E.O.C., Rodriguez, L.C.E., Coomes, D.A., 2022. Forest disturbance and growth processes are reflected in the geographical distribution of large canopy gaps across the Brazilian Amazon. J. Ecol. 110 (12), 2971–2983. https://doi.org/10.1111/1365-2745.14003.

Renaud, J.-P., Vega, C., Durrieu, S., Lisein, J., Magnussen, S., Lejeune, P., Fournier, M., 2017. Stand-level wind damage can be assessed using diachronic photogrammetric canopy height models. Ann. For. Sci. 74 (4), 1–11. https://doi.org/10.1007/s13595-017-0669-3.

Ritter, E., Dalsgaard, L., Einhorn, K.S., 2005. Light, temperature and soil moisture regimes following gap formation in a semi-natural beech-dominated forest in Denmark. For. Ecol. Manag. 206 (1–3), 15–33. https://doi.org/10.1016/j.foreco.2004.08.011.

Ronneberger, O., Fischer, P., Brox, T., 2015. U-net: Convolutional networks for biomedical image segmentation. In: Navab, N., Hornegger, J., Wells, W., Frangi, A. (Eds.), Medical Image Computing and Computer-Assisted Intervention—MICCAI 2015, vol. 9351. Springer, Cham, pp. 234–241. Lecture Notes in Computer Science (),. https://doi.org/10.1007/978-3-319-24574-4_28.

Roussel, J.-R., 2024. lasR: Fast and Pipeable Airborne LiDAR Data Tools. https://github.com/r-lidar/lasR.

Runkle, J.R., 1982. Patterns of disturbance in some old–growth mesic forests of Eastern North America. Ecology 63 (5), 1533–1546. https://doi.org/10.2307/1938878.

Runkle, J.R., 1992. Guidelines and Sample Protocol for Sampling Forest Gaps. Gen. Tech. Rep. PNW-GTR-283. Department of Agriculture, Forest Service, Pacific Northwest Research Station, Portland, OR: U.S. https://doi.org/10.2737/pnw-gtr-283.

Schall, P., Gossner, M.M., Heinrichs, S., Fischer, M., Boch, S., Prati, D., Jung, K., Baumgartner, V., Blaser, S., Böhm, S., Buscot, F., Daniel, R., Goldmann, K., Kaiser, K., Kahl, T., Lange, M., Müller, J., Overmann, J., Renner, S.C., Schulze, E.-D., Sikorski, J., Tschapka, M., Türke, M., Weisser, W.W., Wemheuer, B., Wubet, T., Ammer, C., 2018. The impact of even–aged and uneven–aged forest management on regional biodiversity of multiple taxa in European beech forests. J. Appl. Ecol. 55 (1), 267–278. https://doi.org/10.1111/1365-2664.12950.

Schiefer, F., Kattenborn, T., Frick, A., Frey, J., Schall, P., Koch, B., Schmidtlein, S., 2020. Mapping forest tree species in high resolution UAV-based RGB-imagery by means of convolutional neural networks. ISPRS J. Photogramm. Remote Sens. 170, 205–215. https://doi.org/10.1016/j.isprsjprs.2020.10.015.

Schliemann, S.A., Bockheim, J.G., 2011. Methods for studying treefall gaps: a review. For. Ecol. Manag. 261 (7), 1143–1151. https://doi.org/10.1016/j.foreco.2011.01.011.

Schmitt, M., Hughes, L.H., Qiu, C., Zhu, X.X., 2019. SEN12MS - a curated dataset of georeferenced multi-spectral sentinel-1/2 imagery for deep learning and data fusion. ISPRS Ann. Photogramm. Remote Sens. Spat. Inf. Sci. IV-2/W7, 153–160. https://doi.org/10.5194/isprs-annals-IV-2-W7-153-2019.

Seidel, D., Ammer, C., Puettmann, K., 2015. Describing forest canopy gaps efficiently, accurately, and objectively: new prospects through the use of terrestrial laser scanning. Agr. For. Meteorol. 213, 23–32. https://doi.org/10.1016/j.agrformet.2015.06.006.

Silva, C.A., Valbuena, R., Pinagé, E.R., Mohan, M., Almeida, D.R.A., North Broadbent, E., Jaafar, W.S.W.M., Papa, D., Cardil, A., Klauberg, C., 2019. ForestGapR: an R package for forest gap analysis from canopy height models. Methods Ecol. Evol. 10 (8), 1347–1356. https://doi.org/10.1111/2041-210X.13211.

Solano, F., Modica, G., Praticò, S., Box, O.F., Piovesan, G., 2022. Unveiling the complex canopy spatial structure of a Mediterranean old-growth beech (*Fagus sylvatica* L.) forest from UAV observations. Ecol. Indic. 138, 108807. https://doi.org/10.1016/j.ecolind.2022.108807.

St-Onge, B., Vepakomma, U., Sénécal, J.-F., Kneeshaw, D., Doyon, F., 2014. Canopy gap detection and analysis with airborne laser scanning. In: Maltamo, M., Næsset, E., Vauhkonen, J. (Eds.), Forestry Applications of Airborne Laser Scanning: Concepts and Case Studies. Springer, Netherlands, pp. 419–437. https://doi.org/10.1007/978-94-017-8663-8_21.

Trimble, 2019. MATCH-3DX, MATCH-T DSM Manual for Version 9.2 and Higher.

Vepakomma, U., St-Onge, B., Kneeshaw, D., 2008. Spatially explicit characterization of boreal forest gap dynamics using multi-temporal lidar data. Remote Sens. Environ. 112 (5), 2326–2340. https://doi.org/10.1016/j.rse.2007.10.001.

Vodde, F., Jõgiste, K., Engelhart, J., Frelich, L.E., Moser, W.K., Sims, A., Metslaid, M., 2015. Impact of wind-induced microsites and disturbance severity on tree regeneration patterns: results from the first post-storm decade. For. Ecol. Manag. 348, 174–185. https://doi.org/10.1016/j.foreco.2015.03.052.

Wagner, F.H., Sanchez, A., Tarabalka, Y., Lotte, R.G., Ferreira, M.P., Aidar, M.P.M., Gloor, E., Phillips, O.L., Aragão, L.E.O.C., 2019. Using the U-net convolutional network to map forest types and disturbance in the Atlantic rainforest with very high resolution images. Remote Sens. Ecol. Conserv. 5 (4), 360–375. https://doi.org/10.1002/rse2.111.

Watt, A.S., 1947. Pattern and process in the plant community. J. Ecol. 35 (1/2), 1–22. https://doi.org/10.2307/2256497.

Weinstein, B.G., Marconi, S., Bohlman, S., Zare, A., White, E., 2019. Individual tree-crown detection in RGB imagery using semi-supervised deep learning neural networks. Remote Sens. 11 (11), 1309. https://doi.org/10.3390/rs11111309.

White, J.C., Tompalski, P., Coops, N.C., Wulder, M.A., 2018. Comparison of airborne laser scanning and digital stereo imagery for characterizing forest canopy gaps in coastal temperate rainforests. Remote Sens. Environ. 208, 1–14. https://doi.org/10.1016/j.rse.2018.02.002.

Whitmore, T.C., 1989. Canopy gaps and the two major groups of forest trees. Ecology 70 (3), 536–538. https://doi.org/10.2307/1940195.

Xia, J., Wang, Y., Dong, P., He, S., Zhao, F., Luan, G., 2022. Object-oriented canopy gap extraction from UAV images based on edge enhancement. Remote Sens. 14 (19), 4762. https://doi.org/10.3390/rs14194762.

Zielewska-Büttner, K., Adler, P., Ehmann, M., Braunisch, V., 2016a. Automated detection of Forest gaps in spruce dominated stands using canopy height models derived from stereo aerial imagery. Remote Sens. 8 (3), 175. https://doi.org/10.3390/rs8030175.

Zielewska-Büttner, K., Adler, P., Petersen, M., Braunisch, V., 2016b. Parameters influencing forest gap detection using canopy height models derived from stereo aerial imagery. Publ. DGPF 25, 405–416.